Strongly enhanced exciton-phonon coupling in two-dimensional WSe_2

Luojun Du,[1,2] Mengzhou Liao,[1] Jian Tang,[1] Qian Zhang,[2] Hua Yu,[1] Rong Yang,[1] Kenji Watanabe,[3] Takashi Taniguchi,[3] Dongxia Shi,[1,4,5,*] Qingming Zhang,[1,2] and Guangyu Zhang[1,4,5,6,†]

[1]*Institute of Physics, Chinese Academy of Sciences, Beijing 100190, China*

[2]*Department of Physics, Renmin University of China, Beijing 100872, China*

[3]*Advanced Materials Laboratory, National Institute for Materials Science, 1-1 Namiki, Tsukuba 305-0044, Japan*

[4]*School of Physical Sciences, University of Chinese Academy of Science, Beijing 100190, China*

[5]*Beijing Key Laboratory for Nanomaterials and Nanodevices, Beijing 100190, China*

[6]*Collaborative Innovation Center of Quantum Matter, Beijing 100190, China*

(Received 23 April 2018; revised manuscript received 9 June 2018; published 25 June 2018)

The recently emerging laminar transition metal dichalcogenides provide an unprecedented platform for exploring fascinating layer-dependent properties. Determining the dependence of exciton-phonon coupling (EPC) on dimensionality would set a foundation for these exotic thickness-dependent phenomena. Here we report the observation of layer-dependent EPC between the $A_{1g}(\Gamma)$ phonon and A′ exciton in WSe_2 down to the monolayer limit. Our results uncover that the strength of EPC increases dramatically with a descent of layer thickness. Compared with their bulk counterparts, the strength of EPC in monolayer WSe_2 is enhanced by nearly an order of magnitude. Furthermore, our work demonstrates that the giant EPC in the monolayer plays a prominent role in the exotic interlayer EPC of WSe_2/boron nitride heterostructures. The gigantic EPC in the two-dimensional limit provides a firm basis for understanding and manipulating the peculiar phenomena and novel optoelectronic applications based on atomically thin WSe_2.

DOI: 10.1103/PhysRevB.97.235145

Exciton-phonon coupling (EPC), a fundamental interaction between elementary excitations, plays a vital role in a wide range of properties in condensed-matter physics [1]. For instance, EPC drives the formation of Cooper pairs [2], enables the emergence of superconductivity in iron-based materials [3], favors the Peierls instability [1,4], and dominates photocarrier dynamics [5]. Two-dimensional (2D) transition metal dichalcogenides (TMDCs) have sparked significant attention due to a cornucopia of exotic phenomena [6–9]. Because of the quantum confinement effect, EPC plays a fundamental role in determining the intriguing physics, e.g., phonon-limited electron mobility [10], anti-Stokes emission from trion to neutral exciton [11], strongly enhanced charge density wave transition temperature [12], and EPC-dictated exciton dynamics [13–15].

Since the electronic structures of TMDCs depend strongly on the number of layers [16–18], a strong dependence of EPC on thickness is expected in principle. In fact, it has been shown that the amplitude of EPC in MoS_2 decreases monotonically with a descent of the thickness and only a tiny EPC strength appears in the monolayer limit [19–22]. In contrary to MoS_2, whose $A_{1g}(\Gamma)$ mode is coupled with the A exciton, WSe_2 is found to display atypical EPC [23,24]. The $A_{1g}(\Gamma)$ phonon in WSe_2 is coupled with the A′ exciton instead of the A exciton. What is the layer-dependent EPC between the $A_{1g}(\Gamma)$ phonon and A′ exciton in WSe_2? The influence of layer number on the strength of EPC has not been experimentally explored in WSe_2 thus far. Moreover, recent results demonstrate the fascinating interlayer coupling between boron nitride (hBN) phonons and WSe_2 excitons [25,26]. However, a detailed understanding of the microscopic mechanism that drives such emergent properties has remained elusive. A possible mechanism is that the interlayer EPC in WSe_2/hBN heterostructures is mediated by WSe_2 phonon [26]. If this microscopic theory is true, intralayer EPC in WSe_2 could play a key role in determining the interlayer EPC of WSe_2/hBN heterostructures. Thus, in-depth experiments are highly required to deciphering the EPC of atomically thin WSe_2. Demystifying the EPC of 2D WSe_2 is fundamentally important in both understanding the mechanism of interlayer EPC between WSe_2 and hBN, and searching for novel future electronic applications.

In this paper, we perform off-resonant and resonant Raman scattering on WSe_2 samples with various layer thicknesses to elucidate the layer-dependent EPC. Our experiments reveal that the strength of EPC in WSe_2 associated with the $A_{1g}(\Gamma)$ mode and A′ exciton increases dramatically with a descent of the thickness, in stark contrast to phenomena observed in MoS_2. The giant EPC in atomically thin WSe_2 has profound effects on the interlayer EPC of WSe_2/hBN heterostructures. Our results not only are of fundamental importance in determining the evolution of novel phenomena in 2D limit but also provide guidance for future optoelectronic applications.

Monolayer, bilayer, and few-layer WSe_2 samples were placed on 300-nm SiO_2/Si substrates by mechanical exfoliation from bulk crystal. Figures 1(a)–1(c) show the optical images of typical WSe_2 samples with the number of layers overlaid. Atomically thin WSe_2 flakes were first identified by their interference contrast through the optical microscope and then confirmed by a combination of light absorption,

*Corresponding author: dxshi@iphy.ac.cn

†Corresponding author: gyzhang@aphy.iphy.ac.cn

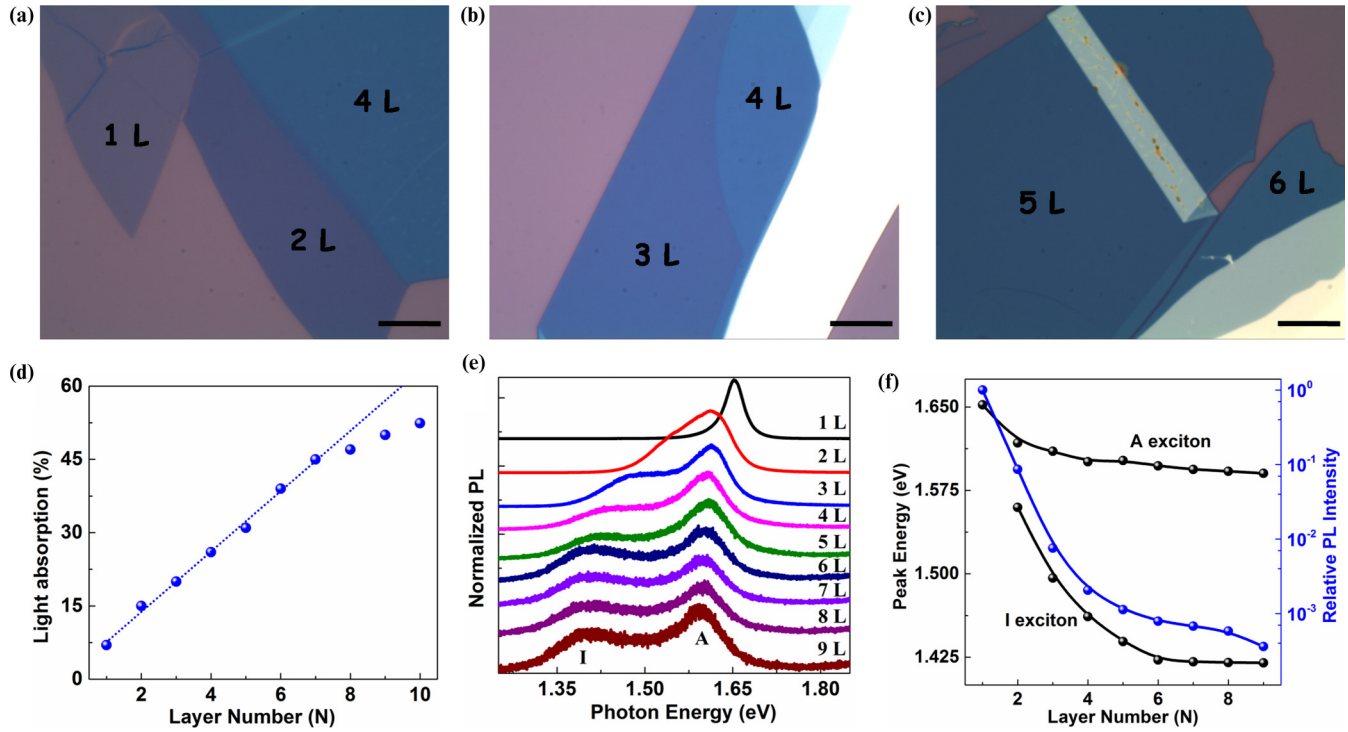

FIG. 1. Microscopy and characterization of WSe_2 with different layers. (a)–(c) White-light microscope images of 1L–6L WSe_2 samples with a $\times 100$ magnification. The scale bars shown in (a)–(c) are 10 μm. (d) Light absorption as a function of the layer number. The dotted line is the linear fitting with a slope of 6%. (e) Normalized PL spectra by the intensity of the A exciton of WSe_2 for layer numbers = 1L–9L. Feature A labels the direct-gap transitions, and I labels the luminescence from an indirect gap interband transition. The spectra were taken under the same conditions using 2.33 eV excitation. (f) Dependence on the layer number of the relative integrated PL intensity normalized by the intensity of the monolayer at 1 (right) and the peak positions of A and I excitons (left).

photoluminescence (PL), and Raman spectroscopy. Optical absorbance (see Supplemental Material [27]) as a function of the layer number is shown in Fig. 1(d). Monolayer WSe_2 possesses a high light absorption of 7% normal incident light, in good agreement with the previous prediction [28]. The light absorption increases linearly with a constant rate of 6% up to 7 L, providing a reliable fingerprint for determining the layer thickness. Figure 1(e) presents the evolution of normalized PL versus the number of layers, exhibiting quite distinct features between mono- and few-layer samples. The PL spectrum of the monolayer consists of a single narrow feature centered at 1.652 eV with FWHM of 36 meV. In stark contrast, few-layer samples display two emission peaks (direct-gap transition A and indirect band-gap luminescence I) [29,30]. The peak positions of A exciton depend weakly on the flake thickness, while I peak quickly shifts toward higher energies with decreasing the number of layers and fades to null at the monolayer limit [the left of Fig. 1(f)]. The strong layer dependence of the indirect gap originates from out-of-plane Se-p_z orbitals at Γ and Q points [18,20], leading to a large interlayer hopping and significant energy change. In addition to the significant difference in the peak energy, PL intensity from the direct interband transition dramatically increases and reaches a maximum at the monolayer limit, more than 1 order of magnitude higher than that of the bilayer and 3 orders of magnitude stronger than that of 9 L [the right of Fig. 1(f)]. Combined with the Raman intensity of the silicon substrate, which has been used to identify the thickness of graphene and TMDCs (Supplemental Material [27]) [31,32], we could identify the layer number of WSe_2 up to 20 L easily.

Although odd layers (D^1_{3h} space group) and even layers (D^3_{3d} space group) belong to different symmetries, we denote all phonons with the irreducible representations of the bulk phase (D^4_{6h} space group) for simplicity. Figure 2(a) shows the nonresonant Raman scattering of WSe_2 with 633-nm excitation. The out-of-plane vibrations of Se atoms [$A_{1g}(\Gamma)$ band] and in-plane breathing mode [$E^1_{2g}(\Gamma)$ band] are close to 250 cm^{-1} and degenerate in monolayer, in fair agreement with the previous study [33]. Being akin to MoS_2 and WS_2, the frequency of the A_{1g} (E^1_{2g}) phonon of WSe_2 blueshifts (redshifts) with increasing the number of layers [Fig. 2(b)] due to the van der Waals interaction and dielectric screening [33,34]. In addition, we can clearly see, from multipeak Lorentzian fittings, that the asymmetrical and broad peak at $\sim 260\ cm^{-1}$ consists of three phonons instead of one phonon [35]: $B_{2g}(M)$ at 256 cm^{-1}, 2LA(M) at 260 cm^{-1}, and 3TA(M) at 262 cm^{-1}, which is usually assigned wrongly to the $A_{1g}(\Gamma)$ mode (see Supplemental Material [27]).

When the incident light (2.33 eV) is in resonance with the A′ exciton of WSe_2 [23,24,33], the Raman scattering shows a significant difference. First, the $A_{1g}(\Gamma)$ and $E^1_{2g}(\Gamma)$ modes cannot be distinguished clearly and only a single peak appears near 250 cm^{-1} [Fig. 2(c)]. To confirm if the single peak near 250 cm^{-1} is from the $A_{1g}(\Gamma)$ mode or $E^1_{2g}(\Gamma)$ phonon, we carried out the polarization-resolved Raman spectroscopy measurements. The intensity at around 250 cm^{-1} in

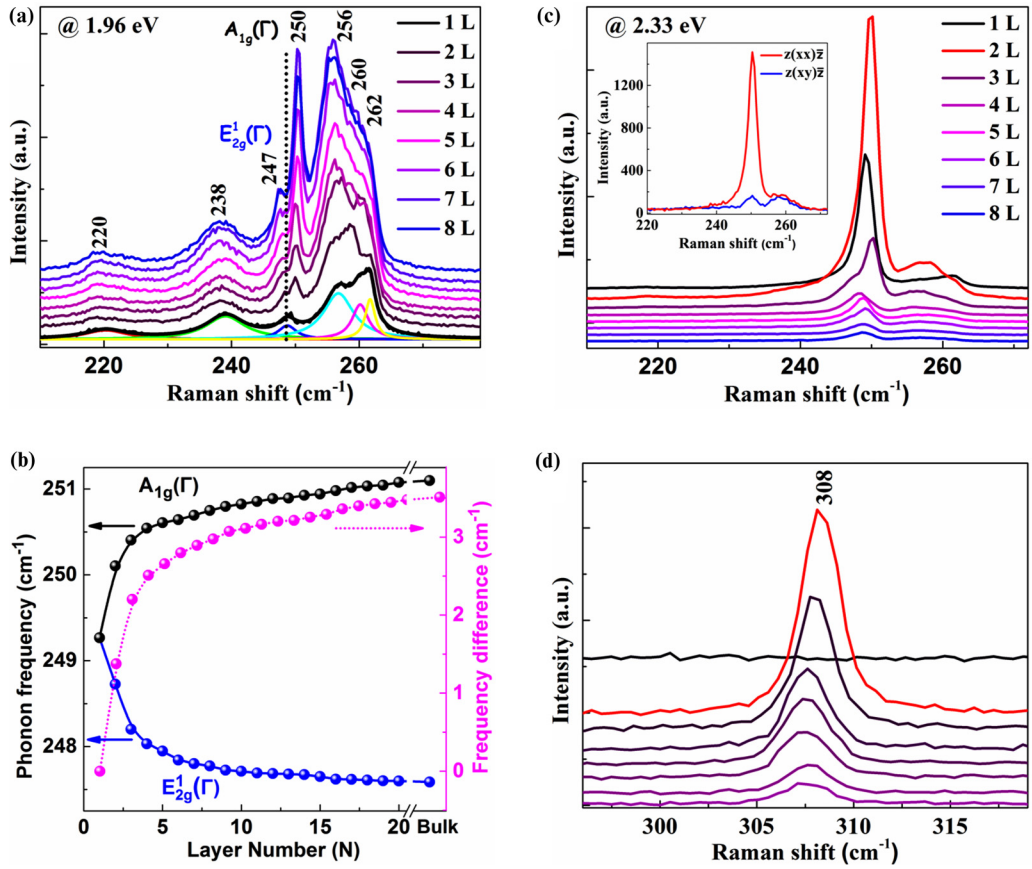

FIG. 2. Resonant and off-resonant Raman spectra of WSe_2. (a) Off-resonant Raman spectra using 633-nm line in the range of 210−280 cm^{-1}. Multipeak Lorentzian fittings of 1L WSe_2 are overlaid. (b) Frequencies of $E^1_{2g}(\Gamma)$ and $A_{1g}(\Gamma)$ Raman modes (left) obtained from Lorentzian fittings of (a) and their difference (right) as a function of layer number. (c), (d) Resonant Raman spectra with 532-nm laser in the range of 210−280 cm^{-1} (c) and 295−320 cm^{-1} (d). Inset in (c) is the Raman spectrum of bilayer WSe_2 obtained in two scattering configurations: copolarized [Z(XX)$\bar{\text{Z}}$] and cross-polarized [Z(XY)$\bar{\text{Z}}$], where Z and $\bar{\text{Z}}$ indicate wave vectors of incident and scattered light.

cross-polarized configuration is much weaker than that in the copolarized configuration [inset in Fig. 2(c)], indicating that the intensity of the $E^1_{2g}(\Gamma)$ mode can be ignored as compared with the $A_{1g}(\Gamma)$ mode [33,36]. Thus, we assign the peak near 250 cm^{-1} to the $A_{1g}(\Gamma)$ phonon when discussing the layer-dependent Raman intensity and EPC below. Second, a new peak at $\sim$ 308 cm^{-1} [Fig. 2(d)], corresponding to the $B^1_{2g}(M)$ mode, is observed for the multilayer (layer number $\geqslant$ 2), resulting from the breaking of Raman selection rules due to resonant Raman processes [36]. The intensity of this mode decreases with increasing the thickness, being an excellent indicator for the number of layers. A series of multiple phonon replica, combinations, and edge phonons of the Brillouin zone are also observed and assigned in Table S3 (Supplemental Material [27]).

Figure 3(c) presents the layer-dependent Raman intensity normalized by the intensity of phonon in bulk counterparts under 1.96 eV excitation (off-resonance). It can be seen that the intensities of all the Raman modes, in close analogy to the case of graphene [37] and MoS_2 [38], increase almost linearly with layer numbers up to 7 L and then decline for even thicker layers. The intensity of all phonons in 7 L is about 18 times higher than those of the bulk. More interestingly, the normalized intensities of all the Raman modes as a function of layer numbers are akin to each other, indicating that the evolution of Raman intensity with the number of layers is attributed to the multilayer interference occurring for both the incident light and emitted Raman radiation [37].

In stark contrast, the intensity of phonons under resonance excitation is quite distinct from off-resonant Raman scattering. Figure 3(d) shows the layer-dependent phonon intensity normalized by Raman intensity in the bulk phase, excited by 2.33 eV radiation on resonance with the A′ exciton [33]. The intensities of all the phonons reach the maximum at the bilayer, and the intensity in the bilayer is much larger than that in the bulk. Especially for the $A_{1g}(\Gamma)$ mode, the intensity in the bilayer is 860 times higher than that in the bulk phase, in good harmony with Raman intensity mapping of $A_{1g}(\Gamma)$ phonons shown in Fig. 3(b). Besides, distinct phonons harbor different layer dependences of normalized Raman intensity, ruling out that the giant Raman intensity in the bilayer stems from optical interference.

To the best of our knowledge, Raman scattering involves an electron-mediated three-step process embodying photon-electron, electron-phonon, and electron-photon interactions. The Raman signal (Raman cross section) can be enhanced significantly when either the incident or inelastically scattered photons are in resonance with the electronic transitions

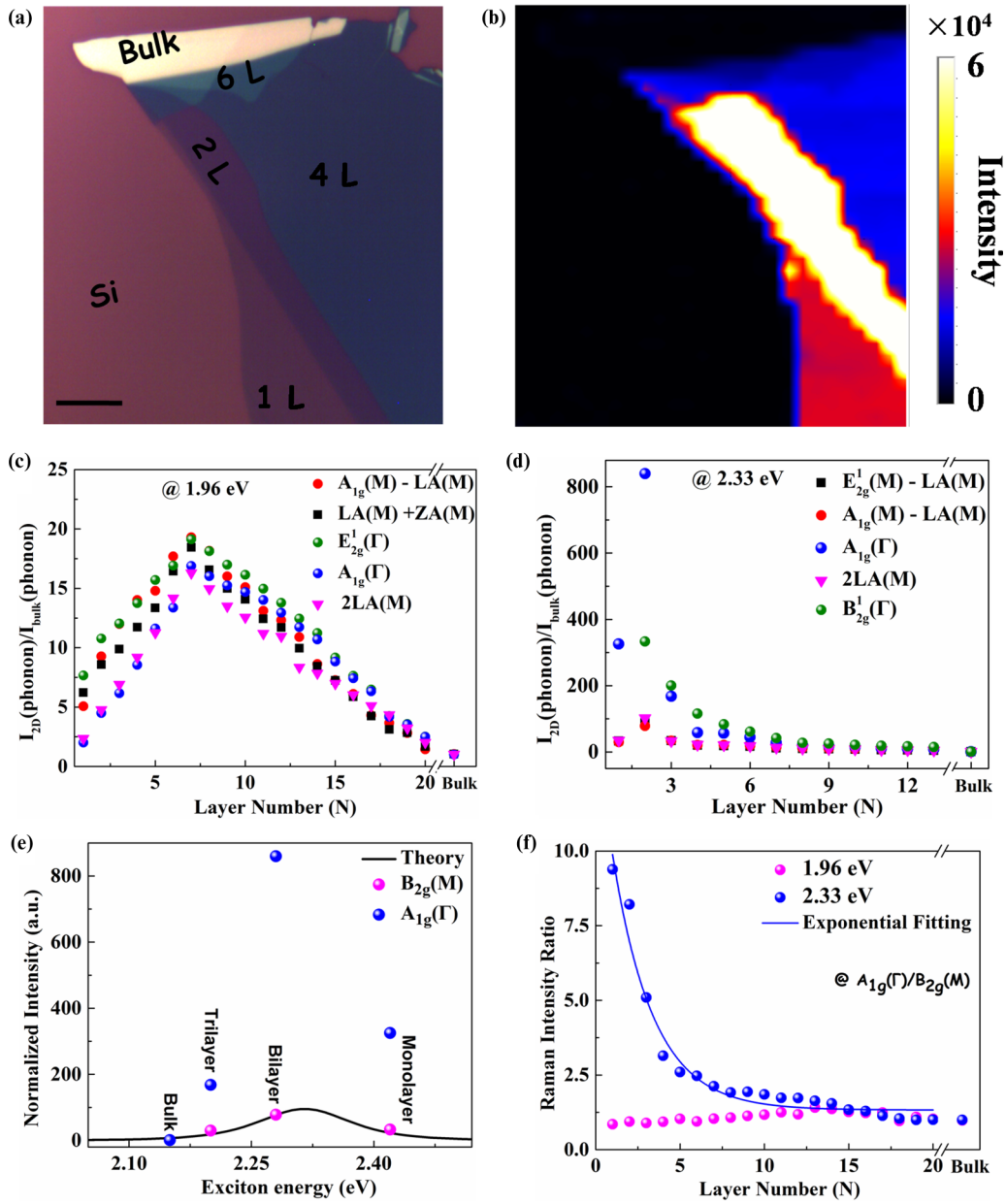

FIG. 3. Layer-dependent exciton-phonon coupling in WSe_2. (a) Optical image of other representative WSe_2 samples on 300-nm-thick SiO_2. We overlay the layer number on top of the corresponding thickness. Scale bar: 15 μm. (b) Raman intensity mapping of the $A_{1g}(\Gamma)$ mode for WSe_2 shown in (a) with 2.33 eV excitation. (c), (d) Raman intensity normalized by the intensity of the bulk as a function of layer number with 1.96 eV excitation (c) and 2.33 eV excitation, on resonance with the A′ exciton (d). (e) Raman intensity normalized by the bulk versus exciton energy. The black theory line is described by Eq. (3). (f) Raman intensity ratio between the $A_{1g}(\Gamma)$ mode and $B_{2g}(M)$ band as a function of layer number.

(excitons). For the first-order Raman process, the Raman intensity is described by the Fermi golden rule for a third-order time-dependent perturbation theory and is given by [19,23]

$$I = \frac{2\pi}{\hbar}\left|\frac{\langle f|H_{e-r}|m_2\rangle\langle m_2|H_{e-ph}|m_1\rangle\langle m_1|H_{e-r}|i\rangle}{(E_L - E_{ex} - i\gamma)(E_L - E_{ex} - E_{ph} - i\gamma)}\right|^2, \quad (1)$$

where $|i\rangle$, $|f\rangle$ and $|m_1\rangle/|m_2\rangle$ are initial, final, and intermediate states, respectively; H_{e-r} and H_{e-ph} are the electron-radiation and electron-phonon interaction Hamiltonians, respectively; E_L, E_{ex}, and E_{ph} are laser energy (2.33 eV), excitonic state (layer-dependent A′ exciton in our case), and phonon energy of the analyzed Raman feature, respectively. And γ represents damping constants related to the lifetimes of the intermediate states. From the denominator of Eq. (1), we could expect that the Raman intensity would reach its maximum when incident energy is in resonance with the energy of the A′ exciton. This is in fair agreement with our results that all the phonons possess the strongest intensity in the bilayer, as the energy of the A′ exciton (2.28 eV) in the bilayer, derived from Refs. [23] and [30], is closest to 2.33 eV.

To obtain the layer-dependent EPC associated with the A′ exciton, we first inspect whether the amplitude of the EPC is the same in distinct thickness or not. If the strength of the EPC

is thickness independent, Eq. (1) could be written

$$I \propto \frac{2\pi}{\hbar}\left|\frac{1}{(E_L - E_{ex} - i\gamma)(E_L - E_{ex} - E_{ph} - i\gamma)}\right|^2. \quad (2)$$

In order to compare with our experimental results, Eq. (2) is normalized by the intensity of the bulk:

$$I_{\text{nor}} = \left|\frac{(2.33 - 2.16 - i\gamma_1)(2.33 - 2.16 - E_{ph} - i\gamma_1)}{(2.33 - E_{ex} - i\gamma_2)(2.33 - E_{ex} - E_{ph} - i\gamma_2)}\right|^2, \quad (3)$$

where 2.16 eV is the energy of the A′ exciton in the bulk, and γ_1 and γ_2 are damping constants of bulk and few-layer WSe_2, respectively. From Ref. [23], it can be known that γ_1 is 0.08. Figure 3(e) and Fig. S5 (Supplemental Material [27]) demonstrate that the intensities of $B_{2g}(M)$, $E^1_{2g}(M)$−LA(M), and $A_{1g}(M)$−LA(M) modes show good agreement with Eq. (3) [theory curve in Fig. 3(e) with γ_2 0.16 and E_{ph} 31 meV], indicating that the EPC between these phonons and the A′ exciton is almost independent of the number of layers. Strikingly, the intensity of the $A_{1g}(\Gamma)$ mode cannot be described by the theory curve at all [Fig. 3(e)], revealing that the strength of EPC between the $A_{1g}(\Gamma)$ phonon and the A′ exciton is strongly dependent on the number of layers.

Although the energy of the A′ exciton is a function of layer numbers, we can eliminate these effects and obtain the layer-dependent EPC between the $A_{1g}(\Gamma)$ phonon and A′ exciton as follows:

$$\frac{I\left(A_{1g}(\Gamma)\right)}{I\left(B_{2g}(M)\right)} \propto \frac{|\langle m_2|H_{e-ph}|m_1\rangle|^2_{A_{1g}(\Gamma)}}{|\langle m_2|H_{e-ph}|m_1\rangle|^2_{B_{2g}(M)}} \propto EPC(A_{1g}(\Gamma)), \quad (4)$$

where $|\langle m_2|H_{e-ph}|m_1\rangle|^2_{A_{1g}(\Gamma)}$ and $|\langle m_2|H_{e-ph}|m_1\rangle|^2_{B_{2g}(M)}$ are the strength of EPC between the A′ exciton and $A_{1g}(\Gamma)$ and $B_{2g}(M)$ modes, respectively. Since EPC between the A′ exciton and the $B_{2g}(M)$ phonon is independent of the layer thickness, the intensity ratio between the $A_{1g}(\Gamma)$ and $B_{2g}(M)$ modes is proportional to the strength of EPC between the A′ exciton and $A_{1g}(\Gamma)$ phonon. Figure 3(f) presents Raman intensity ratio between $A_{1g}(\Gamma)$ and $B_{2g}(M)$ modes versus the number of layers. The resonant Raman intensity ratio between $A_{1g}(\Gamma)$ and $B_{2g}(M)$ modes (blue symbols) drops exponentially as the thickness increases [39], demonstrating that EPC between the $A_{1g}(\Gamma)$ mode and A′ exciton increases dramatically with a descent of the thickness and possesses its maximum in the monolayer limit. This is in good harmony with the results of optical 2D Fourier transform spectroscopy that the EPC of monolayer WSe_2 is a factor of 5–10 larger than that of quasi-2D semiconductor quantum well systems and plays a key role in the intrinsic homogeneous linewidth of excitons [40]. Such a colossal EPC in monolayer WSe_2, being akin to the case of $NbSe_2$ where a strongly enhanced EPC in monolayer leads to a significantly enhanced charge-density-wave transition temperature [12], is of particular significance for exciton dynamics [11,15] and would give rise to a variety of surprising novel quantum phenomena. On the other hand, the Raman intensity ratio between $A_{1g}(\Gamma)$ and $B_{2g}(M)$ modes with off-resonance excitation is thickness independent, as shown in Fig. 3(f) (magenta symbols).

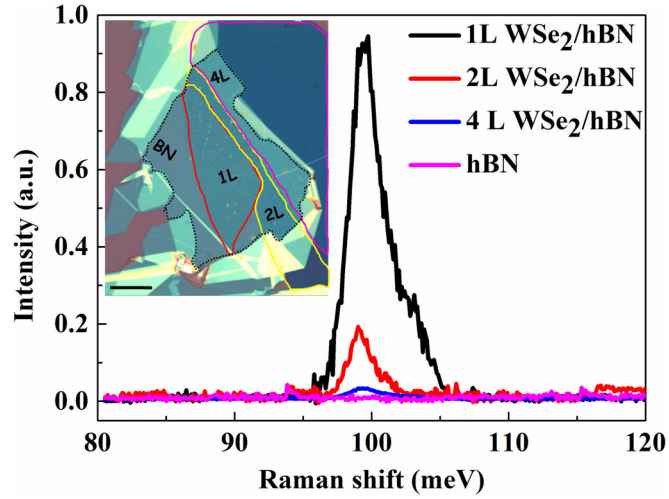

FIG. 4. Layer-dependent interlayer exciton-phonon coupling from 1L WSe_2/hBN (black), 2L WSe_2/hBN (red), 4L WSe_2/hBN (blue), and an adjacent atomically thin hBN (magenta) excited by 2.33 radiation. Inset is the optical micrograph of hBN/WSe_2 heterostructures. Thin hBN with uniform thickness is highlighted by the dashed black line. Monolayer, bilayer, and quadrilayer WSe_2 are highlighted by red, yellow, and magenta lines, respectively. Scale bar: 10 μm.

Recently, extraordinary interlayer coupling between hBN phonons and WSe_2 excitons has been demonstrated in WSe_2/hBN heterostructures. A detailed microscopic mechanism that leads to the interlayer EPC has, however, remained elusive. One of the possible mechanisms is that this exotic interlayer EPC is mediated by WSe_2 phonons [26]. If this is correct, we expect that the intralayer EPC in WSe_2 would play a key role in determining the interlayer EPC of WSe_2/hBN heterostructures. To confirm this view, we covered a thin hBN on WSe_2 by a dry transfer method based on a polydimethylsiloxane (PDMS) stamp [41] and measured the influence of WSe_2 thickness on interlayer EPC of WSe_2/hBN heterostructures. The inset of Fig. 4 presents the white-light microscopic image of monolayer, bilayer, and quadilayer WSe_2 covered by a thin hBN (∼ 6 nm). Figure 4 presents the Raman spectra for 1L WSe_2/hBN (black), 2L WSe_2/hBN (red), 4L WSe_2/hBN (blue), and an atomically thin hBN (magenta) using 532 nm excitation. In stark contrast to pristine hBN, Raman silent hBN ZO mode (99 meV) becomes Raman active in WSe_2/hBN heterostructures, in line with previous findings [25,26]. Strikingly, it can be seen that the intensity of hBN ZO phonons in WSe_2/hBN heterostructures increases sharply with decreasing number of layers and reaches a maximum at the monolayer WSe_2, in good harmony with the giant EPC of WSe_2 monolayers. Our results show unambiguously that the intralayer EPC in WSe_2 is fundamentally important for the exotic interlayer EPC of WSe_2/hBN heterostructures.

In conclusion, we have measured layer-dependent Raman spectroscopy of WSe_2 under both resonant and off-resonant excitations with an A′ exciton. We demonstrate the strength of EPC between $A_{1g}(\Gamma)$ and the A′ exciton in WSe_2 as a function of the number of layers. The EPC in WSe_2 harbors a sharp increase with a descent of the layer thickness. The giant EPC in atomically thin WSe_2 fundamentally determines the interlayer

EPC of WSe_2/hBN heterostructures. Our work provides a firm basis for elaborating the mechanism of the interlayer EPC in WSe_2/hBN heterostructures and will foresee a variety of novel applications in the fields of electronics and optoelectronics.

We acknowledge Feng Wang from UC Berkeley for valuable discussions. G.Y.Z. is grateful for support from the National Key R&D program under Grant No. 2016YFA0300904, the National Science Foundation of China (NSFC, Grant No. 61325021), the Key Research Program of Frontier Sciences of the Chinese Academy of Sciences (CAS, Grant No. QYZDB-SSW-SLH004), and the Strategic Priority Research Program (B) of CAS (Grants No. XDPB06 and No. XDB07010100). D.X.S. is thankful for support from the NSFC through Grants No. 51572289 and No. 61734001.

[1] D. I. Khomskii, *Basic Aspects of the Quantum Theory of Solids: Order and Elementary Excitations* (Cambridge University Press, Cambridge, UK, 2010).

[2] J. Bardeen, L. N. Cooper, and J. R. Schrieffer, Theory of superconductivity, Phys. Rev. **108**, 1175 (1957).

[3] S. Gerber, S.-L. Yang, D. Zhu, H. Soifer, J. A. Sobota, J. J. Lee, T. Jia, B. Moritz, C. Jia, A. Gauthier, Y. Li, D. Leuenberger, Y. Zhang, L. Chaix, W. Li, H. Jang, J.-S. Lee, M. Yi, G. L. Dakovski, S. Song, J. M. Glownia, S. Nelson, K. W. Kim, Y.-D. Chuang, Z. Hussain, R. G. Moore, T. P. Devereaux, W.-S. Lee, P. S. Kirchmann, and Z.-X. Shen, Femtosecond electron-phonon lock-in by photoemission and x-ray free-electron laser, Science **357**, 71 (2017).

[4] O. Dubay, G. Kresse, and H. Kuzmany, Phonon Softening in Metallic Nanotubes by a Peierls-Like Mechanism, Phys. Rev. Lett. **88**, 235506 (2002).

[5] F. Rossi and T. Kuhn, Theory of ultrafast phenomena in photoexcited semiconductors, Rev. Mod. Phys. **74**, 895 (2002).

[6] H. Zeng and X. Cui, An optical spectroscopic study on two-dimensional group-VI transition metal dichalcogenides, Chem. Soc. Rev. **44**, 2629 (2015).

[7] S. Manzeli, D. Ovchinnikov, D. Pasquier, O. V. Yazyev, and A. Kis, 2D transition metal dichalcogenides, Nat. Rev. Mater. **2**, 17033 (2017).

[8] K. F. Mak and J. Shan, Photonics and optoelectronics of 2D semiconductor transition metal dichalcogenides, Nat. Photonics **10**, 216 (2016).

[9] J. R. Schaibley, H. Yu, G. Clark, P. Rivera, J. S. Ross, K. L. Seyler, W. Yao, and X. Xu, Valleytronics in 2D materials, Nat. Rev. Mater. **1**, 16055 (2016).

[10] K. Kaasbjerg, K. S. Thygesen, and K. W. Jacobsen, Phonon-limited mobility in n-type single-layer MoS_2 from first principles, Phys. Rev. B **85**, 115317 (2012).

[11] A. M. Jones, H. Yu, J. R. Schaibley, J. Yan, D. G. Mandrus, T. Taniguchi, K. Watanabe, H. Dery, W. Yao, and X. Xu, Excitonic luminescence upconversion in a two-dimensional semiconductor, Nat. Phys. **12**, 323 (2016).

[12] X. Xi, L. Zhao, Z. Wang, H. Berger, L. Forró, J. Shan, and K. F. Mak, Strongly enhanced charge-density-wave order in monolayer $NbSe_2$, Nat. Nanotechnol. **10**, 765 (2015).

[13] P. Dey, J. Paul, Z. Wang, C. Stevens, C. Liu, A. Romero, J. Shan, D. Hilton, and D. Karaiskaj, Optical Coherence in Atomic-Monolayer Transition-Metal Dichalcogenides Limited by Electron-Phonon Interactions, Phys. Rev. Lett. **116**, 127402 (2016).

[14] C. M. Chow, H. Yu, A. M. Jones, J. R. Schaibley, M. Koehler, D. G. Mandrus, R. Merlin, W. Yao, and X. Xu, Phonon-assisted oscillatory exciton dynamics in monolayer $MoSe_2$, NPJ 2D Mater. Appl. **1**, 33 (2017).

[15] G. Wang, M. Glazov, C. Robert, T. Amand, X. Marie, and B. Urbaszek, Double Resonant Raman Scattering and Valley Coherence Generation in Monolayer WSe_2, Phys. Rev. Lett. **115**, 117401 (2015).

[16] K. F. Mak, C. Lee, J. Hone, J. Shan, and T. F. Heinz, Atomically Thin: A new Direct-Gap Semiconductor, Phys. Rev. Lett. **105**, 136805 (2010).

[17] A. Splendiani, L. Sun, Y. Zhang, T. Li, J. Kim, C.-Y. Chim, G. Galli, and F. Wang, Emerging photoluminescence in monolayer MoS_2, Nano Lett. **10**, 1271 (2010).

[18] G.-B. Liu, D. Xiao, Y. Yao, X. Xu, and W. Yao, Electronic structures and theoretical modelling of two-dimensional group-VIB transition metal dichalcogenides, Chem. Soc. Rev. **44**, 2643 (2015).

[19] B. R. Carvalho, L. M. Malard, J. M. Alves, C. Fantini, and M. A. Pimenta, Symmetry-Dependent Exciton-Phonon Coupling in 2D and Bulk MoS_2 Observed by Resonance Raman Scattering, Phys. Rev. Lett. **114**, 136403 (2015).

[20] L. Du, T. Zhang, M. Liao, G. Liu, S. Wang, R. He, Z. Ye, H. Yu, R. Yang, D. Shi, Y. Yao, and G. Zhang, Temperature-driven evolution of critical points, interlayer coupling, and layer polarization in bilayer MoS_2, Phys. Rev. B **97**, 165410 (2018).

[21] N. Scheuschner, O. Ochedowski, M. Schleberger, and J. Maultzsch, Resonant Raman profiles and μ-photoluminescence of atomically thin layers of molybdenum disulfide, Phys. Status Solidi B **249**, 2644 (2012).

[22] H. Li, Q. Zhang, C. C. R. Yap, B. K. Tay, T. H. T. Edwin, A. Olivier, and D. Baillargeat, From bulk to monolayer MoS_2: Evolution of Raman scattering, Adv. Funct. Mater. **22**, 1385 (2012).

[23] E. del Corro, H. Terrones, A. Elias, C. Fantini, S. Feng, M. A. Nguyen, T. E. Mallouk, M. Terrones, and M. A. Pimenta, Excited excitonic states in 1L, 2L, 3L, and bulk WSe_2 observed by resonant Raman spectroscopy, ACS Nano **8**, 9629 (2014).

[24] E. del Corro, A. Botello-Méndez, Y. Gillet, A. L. Elias, H. Terrones, S. Feng, C. Fantini, Daniel Rhodes, N. Pradhan, L. Balicas, X. Gonze, J.-C. Charlier, M. Terrones, and M. A. Pimenta, Atypical exciton—Phonon interactions in WS_2 and WSe_2 monolayers revealed by resonance Raman spectroscopy, Nano Lett. **16**, 2363 (2016).

[25] C. Jin, J. Kim, J. Suh, Z. Shi, B. Chen, X. Fan, M. Kam, K. Watanabe, T. Taniguchi, S. Tongay, A. Zettl, J. Wu, and F. Wang, Interlayer electron–phonon coupling in WSe_2/hBN heterostructures, Nat. Phys. **13**, 127 (2017).

[26] C. M. Chow, H. Yu, A. M. Jones, J. Yan, D. G. Mandrus, T. Taniguchi, K. Watanabe, W. Yao, and X. Xu, Unusual exciton−phonon interactions at van der Waals engineered interfaces, Nano Lett. **17**, 1194 (2017).

[27] See Supplemental Material at http://link.aps.org/supplemental/10.1103/PhysRevB.97.235145 for details on sample preparation and characterization, Raman intensity of the 520.7 cm^{-1} mode, controversy on the assignment of the $A_{1g}(\Gamma)$ band and peak at 260 cm^{-1}, multipeak Lorentzian fittings of the 260 cm^{-1} mode, layer-dependent Raman spectra, Raman peak assignments, exciton energy-dependent Raman intensity, and Raman spectra of WSe_2/hBN. This includes Refs. [23,24,26,29,30,33,36,42–50].

[28] M. Bernardi, M. Palummo, and J. C. Grossman, Extraordinary sunlight absorption and one nanometer thick photovoltaics using two-dimensional monolayer materials, Nano Lett. **13**, 3664 (2013).

[29] H. Zeng, G-B. Liu, J. Dai, Y. Yan, B. Zhu, R. He, L. Xie, S. Xu, X. Chen, W. Yao, and X. Cui, Optical signature of symmetry variations and spin-valley coupling in atomically thin tungsten dichalcogenides, Sci. Rep. **3**, 1608 (2013).

[30] W. Zhao, Z. Ghorannevis, L. Chu, M. Toh, C. Kloc, P.-H. Tan, and G. Eda, Evolution of electronic structure in atomically thin sheets of WS_2 and WSe_2, ACS Nano **7**, 791 (2012).

[31] X.-L. Li, X.-F. Qiao, W.-P. Han, X. Zhang, Q.-H. Tan, T. Chen, and P.-H. Tan, Determining layer number of two-dimensional flakes of transition-metal dichalcogenides by the Raman intensity from substrates, Nanotechnology **27**, 145704 (2016).

[32] X.-L. Li, X.-F. Qiao, W.-P. Han, Y. Lu, Q.-H. Tan, X.-L. Liu, and P.-H. Tan, Layer number identification of intrinsic and defective multilayered graphenes up to 100 layers by the Raman mode intensity from substrates, Nanoscale **7**, 8135 (2015).

[33] W. Zhao, Z. Ghorannevis, K. K. Amara, J. R. Pang, M. Toh, X. Zhang, C. Kloc, P. H. Tan, and G. Eda, Lattice dynamics in mono- and few-layer sheets of WS_2 and WSe_2, Nanoscale **5**, 9677 (2013).

[34] A. Molina-Sánchez and L. Wirtz, Phonons in single-layer and few-layer MoS_2 and WS_2, Phys. Rev. B **84**, 155413 (2011).

[35] X. Zhang, X.-F. Qiao, W. Shi, J.-B. Wu, D.-S. Jiang, and P.-H. Tan, Phonon and Raman scattering of two-dimensional transition metal dichalcogenides from monolayer, multilayer to bulk material, Chem. Soc. Rev. **44**, 2757 (2015).

[36] X. Luo, Y. Zhao, J. Zhang, M. Toh, C. Kloc, Q. Xiong, and S. Y. Quek, Effects of lower symmetry and dimensionality on Raman spectra in two-dimensional WSe_2, Phys. Rev. B **88**, 195313 (2013).

[37] Y. Wang, Z. Ni, Z. Shen, H. Wang, and Y. Wu, Interference enhancement of Raman signal of graphene, Appl. Phys. Lett. **92**, 043121 (2008).

[38] C. Lee, H. Yan, L. E. Brus, T. F. Heinz, J. Hone, and S. Ryu, Anomalous lattice vibrations of single- and few-layer MoS_2, ACS Nano **4**, 2695 (2010).

[39] It should be noted that the exponential fitting in Fig. 3(f) is intended to show that the EPC increases dramatically with a descent of layer thickness rather than demystifying the precise form for the layer-dependent EPC. The precise form is beyond the present study and needs further quantitative studies to elaborate.

[40] G. Moody, C. K. Dass, K. Hao, C-H. Chen, L-J. Li, A. Singh, K. Tran, G. Clark, X. Xu, G. Berghäuser, E. Malic, A. Knorr, and X. Li, Intrinsic homogeneous linewidth and broadening mechanisms of excitons in monolayer transition metal dichalcogenides, Nat. Commun. **6**, 8315 (2015).

[41] X. Cui, G.-H. Lee, Y. D. Kim, G. Arefe, P. Y. Huang, C.-H. Lee, D. A. Chenet, X. Zhang, L. Wang, F. Ye, F. Pizzocchero, B. S. Jessen, K. Watanabe, T. Taniguchi, D. A. Muller, T. Low, P. Kim, and J. Hone, Multi-terminal transport measurements of MoS_2 using a van der Waals heterostructure device platform, Nat. Nanotechnol. **10**, 534 (2015).

[42] H. Li, J. Wu, X. Huang, G. Lu, J. Yang, X. Lu, Q. Xiong, and H. Zhang, Rapid and reliable thickness identification of two-dimensional nanosheets using optical microscopy, ACS Nano **7**, 10344 (2013).

[43] D. Mead and J. Irwin, Long wavelength optic phonons in WSe_2, Can. J. Phys. **55**, 379 (1977).

[44] P. Tonndorf, R. Schmidt, P. Böttger, X. Zhang, J. Börner, A. Liebig, M. Albrecht, C. Kloc, O. Gordan, D. R. T. Zahn, S. M. de Vasconcellos, and R. Bratschitsch, Photoluminescence emission and Raman response of monolayer MoS_2, $MoSe_2$, and WSe_2, Opt. Express **21**, 4908 (2013).

[45] S.-Y. Chen, C. Zheng, M. S. Fuhrer, and J. Yan, Helicity-resolved Raman scattering of MoS_2, $MoSe_2$, WS_2, and WSe_2 atomic layers, Nano Lett. **15**, 2526 (2015).

[46] H. Li, G. Lu, Y. Wang, Z. Yin, C. Cong, Q. He, L. Wang, F. Ding, T. Yu, and H. Zhang, Mechanical exfoliation and characterization of single- and few-layer nanosheets of WSe_2, TaS_2, and $TaSe_2$, Small **9**, 1974 (2013).

[47] H. Sahin, S. Tongay, S. Horzum, W. Fan, J. Zhou, J. Li, J. Wu, and F. Peeters, Anomalous Raman spectra and thickness-dependent electronic properties of WSe_2, Phys. Rev. B **87**, 165409 (2013).

[48] D. J. Late, S. N. Shirodkar, U. V. Waghmare, V. P. Dravid, and C. Rao, Thermal expansion, anharmonicity and temperature-dependent Raman spectra of single- and few-Layer $MoSe_2$ and WSe_2, Chem. Phys. Chem. **15**, 1592 (2014).

[49] Y. Zhao, X. Luo, H. Li, J. Zhang, P. T. Araujo, C. K. Gan, J. Wu, H. Zhang, S. Y. Quek, M. S. Dresselhaus, and Q. Xiong, Interlayer breathing and shear modes in few-trilayer MoS_2 and WSe_2, Nano Lett. **13**, 1007 (2013).

[50] H. Jeong, H. M. Oh, A. Gokarna, H. Kim, S. J. Yun, G. H. Han, M. S. Jeong, Y. H. Lee, and G. Lerondel, Integrated freestanding two-dimensional transition metal dichalcogenides, Adv. Mater. **29**, 1700308 (2017).